

Neural-network quantum state study of the long-range antiferromagnetic Ising chain

Jicheol Kim,¹ Dongkyu Kim,^{1,2} and Dong-Hee Kim^{1,*}

¹*Department of Physics and Photon Science, Gwangju Institute of Science and Technology, Gwangju 61005, Korea*

²*Kakao Corporation, Pangyo, Gyeonggi 13529, Korea*

We investigate quantum phase transitions in the transverse field Ising chain with algebraically decaying long-range (LR) antiferromagnetic interactions using the variational Monte Carlo method with the restricted Boltzmann machine employed as a trial wave function ansatz. First, we measure the critical exponents and the central charge through the finite-size scaling analysis, verifying the contrasting observations in the previous tensor network studies. The correlation function exponent and the central charge deviate from the short-range (SR) Ising values at a small decay exponent α_{LR} , while the other critical exponents examined are very close to the SR Ising exponents regardless of α_{LR} examined. However, in the further test of the critical Binder ratio, we find that the universal ratio of the SR limit does not hold for $\alpha_{\text{LR}} < 2$, implying a deviation in the criticality. On the other hand, we find evidence of the conformal invariance breakdown in the conformal field theory (CFT) test of the correlation function. The deviation from the CFT description becomes more pronounced as α_{LR} decreases, although a precise breakdown threshold is yet to be determined.

I. INTRODUCTION

Artificial neural networks and machine learning have been influencing the paradigm of physics research with a growing number of applications on various subjects, including phase transitions and critical phenomena in classical and quantum many-body systems [1–4]. In particular, the representation of a quantum wave function by a neural network [5] provides an alternative numerical platform combined with the variational Monte Carlo (VMC) method to find the ground state of a many-body Hamiltonian. The neural-network quantum state (NQS) has extended its area of applications to the Fermi and Bose Hubbard models [6, 7], real-time dynamics [5, 8–10], open quantum systems [11–14], quantum state tomography [15, 16], frustrated systems [17–23], and *ab initio* simulations of molecules [24–26]. The NQS ansatz offers the high expressive capacity often measured in terms of entanglement scaling [27–31], proposing a complementary tool to conventional numerical methods for studying quantum criticality.

In this paper, we investigate quantum phase transitions in the transverse field Ising chain (TFIC) with algebraically decaying long-range (LR) antiferromagnetic (AF) interactions by employing the NQS ansatz for the VMC calculations. LR-interacting quantum systems have attracted growing attention, both theoretical and experimental [32]. The trapped-ion quantum simulation [33] realized the TFIC Hamiltonian with an LR interaction that maps to the form of $1/r^{\alpha_{\text{LR}}}$ with a tunable exponent α_{LR} , providing a controllable experimental platform to study quantum phase transitions at and out of equilibrium [34–36]. The nearest-neighbor-interacting short-range (SR) TFIC is a textbook example of quantum critical behavior in one dimension that belongs to the universality class of the classical two-dimensional (2D) Ising model [37]. However, such quantum-classical correspondence to the universality of critical phenomena becomes nontrivial in the presence of LR interactions. A central question of how criticality depends on α_{LR} is still an active subject of various numerical and analytical

studies [32, 38–65].

We revisit this question on the AF side of the LR interactions for TFIC, where the breakdown of the Ising class in the critical ground state seems to be very different from what is established in the ferromagnetic (FM) counterpart [49–54, 59–61]. Because an exact solution is not available, constructing the picture of how its criticality deviates from the Ising class as α_{LR} decreases relies primarily on the collection of numerical observations. Despite various numerical studies characterizing the quantum phase transition in AF-LR-TFIC at equilibrium [56–60, 62] and out of equilibrium [59, 63], the picture remains incomplete in some parts, which requires more numerical evidence for clarification. Using the restricted Boltzmann machine (RBM) for the NQS ansatz [5], we consider the moments of staggered magnetization including the order parameter and the Binder ratio, the two-point correlation function, and the entanglement entropy to examine the present picture and improve the characterization of the phase transition with increasing LR influences along the critical line.

We begin with brief reviews of previous results on the characterization of the criticality. The first study of AF-LR-TFIC [56] using the time-dependent variational principle (TDVP) found a phase transition for all $\alpha_{\text{LR}} > 0$, where it turned out that the critical exponent of the correlation function decreases from the SR Ising value for $\alpha_{\text{LR}} \lesssim 2$. A significant increase in the central charge from the SR Ising value of $1/2$ was observed for $\alpha_{\text{LR}} \lesssim 1$ in the TDVP [56] and density matrix renormalization group (DMRG) [57] calculations, based on which the breakdown of conformal invariance was proposed [57]. However, more studies are needed because the central charge is not a sufficient indicator of conformal invariance [66]. While we focus on the critical ground state, a violation of the area law for the entanglement entropy was observed in the offcritical area [56, 57, 62], and it was shown that the area law of the noncritical ground state holds for $\alpha_{\text{LR}} > 2$ [67].

On the other hand, contrasting evidence was found in the other DMRG calculations [58, 59], where the estimates of the critical exponents $\nu \simeq 1$ and $\beta \simeq 1/8$ and the dynamic exponent $z \simeq 1$ were in agreement with the SR Ising values for all examined α_{LR} between 0.4 and 3. However, these DMRG estimates of the critical exponents have not been fully verified

* dongheekim@gist.ac.kr

in different approaches. Linked cluster expansion calculations [60] reported $\nu = 1.7(5)$ for $\alpha_{\text{LR}} = 2$ while $\nu \approx 1$ for $\alpha_{\text{LR}} = 9/4$. Previous quantum Monte Carlo (QMC) calculations with stochastic series expansion [61] provided lower values of ν and β in its examined range of $\alpha_{\text{LR}} \geq 2$. While partial disagreements exist between these previous estimates, the TDVP and DMRG results together suggest an interesting possibility that some of the exponents can still be very close to the SR Ising values even for a small α_{LR} where the central charge indicates a deviation, raising the need for verification with a different numerical approach.

Apart from the question about criticality at a small α_{LR} , another issue we want to address is the possibility of conformal invariance breakdown that may occur below a certain value of α_{LR} . The scenario of conformal invariance breakdown was also proposed in the study of the Kitaev chain with LR pairing [64, 65] which becomes equivalent to the Ising chain in the SR limit. Along the critical line of a positive chemical potential, the conformal symmetry is broken for $\alpha_{\text{LR}} < 2$ in the effective action while the Ising exponent β is unchanged in the test of a quantity that corresponds to the Ising order parameter in the SR limit. Although there is no rigorous mapping between the Kitaev and Ising chains at finite α_{LR} , their empirical similarity motivates us to consider the possibility that the same phenomenon could occur in the AF-LR-TFIC.

Detecting the breakdown of conformal invariance must go beyond the test of the central charge. As discussed in Ref. [66], the central charge measured from the entanglement entropy is not a sufficient tool to examine conformal invariance because the logarithmic system-size scaling behavior of the entanglement entropy is not exclusive to conformal invariance. A criterion must be set based on a behavior or quantity fully restricted by conformal field theory (CFT). The scaling and functional form of the correlation function in cylindrical geometry was proposed as a strict indicator [66], which we use in this work to examine conformal invariance.

Our VMC+RBM calculations investigate these questions about criticality and conformal invariance. First, we examine the contrasting evidence from the previous TDVP and DMRG studies [56–59]. In the finite-size scaling (FSS) analysis of the order parameter, we find that the critical exponents ν , β , and γ are indeed very close to the SR Ising values for our examined range of $0.5 \leq \alpha_{\text{LR}} \leq 3$. In contrast, the correlation function exponent and the central charge exhibit deviations from the SR Ising values for $\alpha_{\text{LR}} \lesssim 2$ and $\alpha_{\text{LR}} \lesssim 1$, respectively. These observations verify the previous results. However, the change of the criticality is inconclusive in these contrasting behaviors of the measured exponents, and as discussed above, the deviation of the central charge is not sufficient to claim the breakdown of conformal invariance.

We thus provide additional tests for the Ising criticality and the breakdown of conformal invariance, examining the universal Binder ratio and the CFT description of the correlation function, respectively. It turns out that the critical Binder ratio [42] becomes increasingly different from the universal ratio of the 2D Ising model as α_{LR} decreases below 2, indicating the deviation from the criticality of the SR limit. In the CFT test of the correlation function, we find evidence of the con-

formal invariance breakdown from a mismatch between the CFT description and our measurement, which becomes very pronounced for $\alpha_{\text{LR}} < 2$. However, the slope of the scaled correlation function [66] appears to remain small but nonvanishing for $\alpha_{\text{LR}} \geq 2$. This raises the possibility the breakdown threshold of conformal invariance in the AF-LR-TFIC may differ from the threshold discussed in the Kitaev chain.

This paper is organized as follows. The AF-LR-TFIC model Hamiltonian and the details of the VMC+RBM calculations are described in Sec. II. The previous estimates of the critical exponents and the central charge are verified through Sec. III A, Sec. III B, and Sec. III C, which is followed by our tests using different methods. In Sec. III D, the test for the Ising universality using the Binder ratio is given. In Sec. III E, the CFT test of the correlation function is given to identify the conformal invariance breakdown. Conclusions are given in Sec. IV.

II. MODEL AND VMC+RBM CALCULATIONS

We consider the AF-LR-TFIC Hamiltonian [56] given as

$$\hat{H} = \sin \theta \sum_{i < j} J_{ij} \hat{\sigma}_i^x \hat{\sigma}_j^x + \cos \theta \sum_i \hat{\sigma}_i^z, \quad (1)$$

where θ is in the range of $0 < \theta < \pi/2$ for the AF coupling, and the site indices i and j run from 1 to L in the chain of length L . We impose PBC as the boundary conditions that are necessary for the test of the CFT description of the correlation function constructed in a cylindrical space-time geometry. In the implementation of the algebraically decaying LR interaction under PBC, we choose to write J_{ij} with a range cutoff that increases with the system size L by adopting the formulation used in the LR-Kitaev chain [64, 65] as

$$J_{ij} = \begin{cases} |i - j|^{-\alpha_{\text{LR}}} & \text{for } |i - j| < L/2, \\ (L - |i - j|)^{-\alpha_{\text{LR}}} & \text{for } |i - j| > L/2. \end{cases} \quad (2)$$

We choose RBM as an ansatz of a trial wave function for VMC simulations to find an approximate ground state [5]. A trial state can be written as $|\Psi\rangle = \sum_{\mathbf{s}} \Psi(\mathbf{s}; \mathcal{W}) |\mathbf{s}\rangle$ with the visible variables $\mathbf{s} = (s_1, s_2, \dots, s_L)$ of RBM, where s_i indicates σ_i^x for the $\hat{\sigma}^x$ -basis representation of the given Hamiltonian. We impose the translation symmetry under PBC to reduce the number of variational parameters. Following the procedures of Ref. [5], after integrating out the hidden layer, one can express the RBM wave function as

$$\Psi(\mathbf{s}; \mathcal{W}) = e^{a \sum_{j=1}^L s_j} \prod_{m=1}^L \prod_{i=1}^{n_h} \cosh \left[b_i + \sum_{j=1}^L W_{ij} T_m(s_j) \right], \quad (3)$$

where the translation operator T is defined as $T_m(s_j) = s_{j+m}$ with periodicity $s_{j+L} = s_j$, and n_h is the number of filters given for the symmetry. On a diagram of RBM, one may illustrate the hidden layer with $N_h = Ln_h$ neurons with L -fold degeneracy of the neural variables enforcing the translation invariance. In Eq. (3), there are $(1 + n_h + Ln_h)$ RBM parameters of $\mathcal{W} \equiv \{a, \mathbf{b}, \mathbf{W}\}$ to be optimized using the VMC

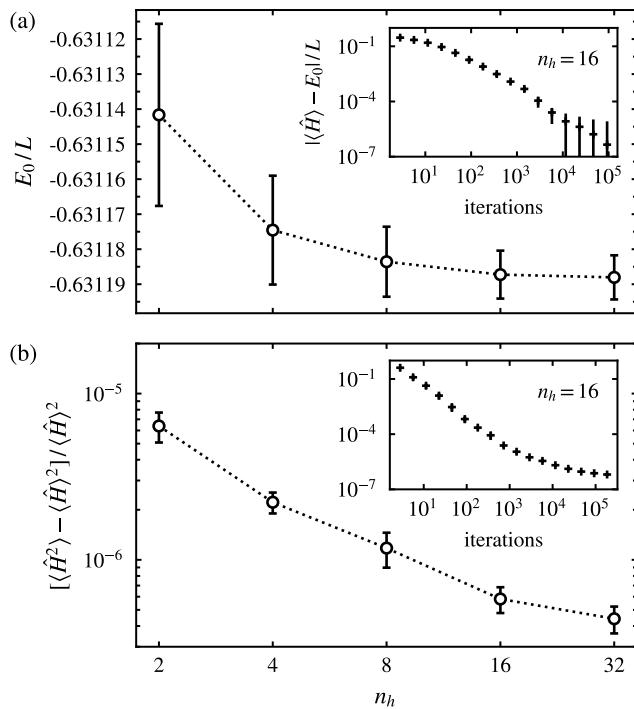


FIG. 1. Convergence test of the RBM wave function in the VMC search for the ground state. The case with the system of the size $L = 64$ for $\alpha_{LR} = 0.5$ is shown for example. The estimates of (a) energy density E_0/L and (b) relative variance $(\langle \hat{H}^2 \rangle - \langle \hat{H} \rangle^2) / \langle \hat{H} \rangle^2$ measured after 2×10^5 iterations are plotted as a function of n_h . The insets show the same quantities for a fixed number of filters $n_h = 16$ monitored during the iterations of the parameter updates. The data points in the insets represent the averages measured in the logarithmic bins of iteration numbers. The error bars are measured with ten independent RBM wave function samples.

method. We adopt complex-valued parameters as suggested in Ref. [5] for better convergence, although the TFIC Hamiltonian is stoquastic [68]. We initialize the RBM by setting $a = 0$ and assigning Gaussian random numbers with zero mean and variance of $1/(Ln_h)$ to \mathbf{b} and \mathbf{W} .

In VMC calculations, we optimize the RBM parameters using the stochastic reconfiguration method to construct the natural gradient [69–71]. This method can be described as the imaginary-time evolution of a trial state, providing a new state projected in the space of $\{|\Psi\rangle, \partial_1|\Psi\rangle, \partial_2|\Psi\rangle, \dots\}$, where $\partial_i|\Psi\rangle \equiv \frac{\partial|\Psi\rangle}{\partial\mathcal{W}_i}$. These procedures propose an update of the variational parameter as $\mathcal{W}_i^{\text{new}} = \mathcal{W}_i^{\text{old}} + \mu\delta\mathcal{W}_i$, where $\delta\mathcal{W}_i$ is determined by solving the linear equation $\mathbf{S}\delta\mathcal{W} = -\mathbf{f}$. The essential numerical procedures are to evaluate the overlap matrix \mathbf{S} and the force vector \mathbf{f} ,

$$S_{ij} = \langle \Delta_i^* \Delta_j \rangle_{\text{mc}} - \langle \Delta_i^* \rangle_{\text{mc}} \langle \Delta_j \rangle_{\text{mc}}, \quad (4)$$

$$f_i = \langle \Delta_i^* E_{\text{loc}} \rangle_{\text{mc}} - \langle \Delta_i^* \rangle_{\text{mc}} \langle E_{\text{loc}} \rangle_{\text{mc}}, \quad (5)$$

where the derivative Δ_i and the local energy E_{loc} are

$$\Delta_i \equiv \frac{\partial_i \Psi(\mathbf{s}; \mathcal{W})}{\Psi(\mathbf{s}; \mathcal{W})} \quad \text{and} \quad E_{\text{loc}} \equiv \sum_{\mathbf{s}'} \langle \mathbf{s} | \hat{H} | \mathbf{s}' \rangle \frac{\Psi(\mathbf{s}'; \mathcal{W})}{\Psi(\mathbf{s}; \mathcal{W})}. \quad (6)$$

The expression $\langle A \rangle_{\text{mc}} \equiv \sum_{\mathbf{s}} P(\mathbf{s}) A(\mathbf{s})$ denotes the Monte Carlo (MC) measurement of $A(\mathbf{s})$ with probability $P(\mathbf{s}) \propto |\Psi(\mathbf{s}; \mathcal{W})|^2$. We use the conjugate gradient algorithm with the Jacobi preconditioner to solve the linear equation without explicitly storing the \mathbf{S} matrix following the cost-reducing recipe of Ref. [71]. For numerical stability, we use the regularization scheme introduced in Ref. [5], where at the p th iteration, S_{ij} is replaced by $S_{ij}(1 + \lambda_p \delta_{ij})$ with $\lambda_p = \max(\lambda_0 b^p, \lambda_{\text{min}})$. We use the parameters $\lambda_0 = 100$, $b = 0.9$, and $\lambda_{\text{min}} = 0.01$. The learning rate μ is initially set to 0.1 and increased by 0.1 for every 10000 iterations until it becomes unity.

We monitor the convergence of $|\Psi\rangle$ to the ground state by evaluating $\langle \hat{H} \rangle$ and the relative variance defined as

$$\tilde{\sigma}_E \equiv \frac{\langle \hat{H}^2 \rangle - \langle \hat{H} \rangle^2}{\langle \hat{H} \rangle^2}. \quad (7)$$

The relative variance $\tilde{\sigma}_E$ should be precisely zero when $|\Psi\rangle$ becomes an exact eigenstate. However, in practice, it does not decrease below a certain value in VMC simulations. Probable systematic causes may include the limited expressive power of a finite-size neural network with a finite n_h , despite the universal approximation theorem, and the stochastic fluctuations in MC measurements that can affect the linear solver.

Figure 1 presents an example of the convergence test performed at the critical point in the system of size $L = 64$ for the LR exponent $\alpha_{LR} = 0.5$. Convergence tends to slow down as α_{LR} decreases in this LR-AF system. At the critical point, it typically takes about an order of 10^5 iterations until the energy and variance become saturated within the scale of their fluctuations over the iterations. We find that the accuracy level indicated by $\tilde{\sigma}_E$ after saturation depends essentially on the number of filters n_h . In our VMC calculations for the ground state, we set the convergence criterion as $\tilde{\sigma}_E < 10^{-6}$, which, for example, is achieved for $n_h > 8$ in Fig. 1. In our tests, $n_h = 16$ suffices to satisfy $\tilde{\sigma}_E < 10^{-6}$ for system sizes up to $L = 128$ in the range of α_{LR} that we consider.

III. RESULTS AND DISCUSSIONS

Using the RBM wave function $\Psi(\mathbf{s})$ obtained in the VMC optimizations at a given θ , we measure the moments of staggered magnetization including the AF order parameter, the two-point correlation function, and the second Rényi entanglement entropy. For a given RBM sample, the MC averages are calculated with 4×10^8 configurations of \mathbf{s} sampled from the probability distribution $P(\mathbf{s}) \propto |\Psi(\mathbf{s})|^2$ using the Metropolis algorithm. We obtain ten RBM wave function samples from independent VMC calculations. We find that the standard error of the measurement based on one RBM sample is typically smaller than the sample-to-sample fluctuations, and thus, we estimate the error bar by the standard deviation of the measurements over the RBM samples.

In this section, we first present the FSS analysis to estimate the critical exponents and the central charge for comparison with the previous TDVP and DMRG results. Then, we proceed to present our additional tests of the universal Binder ratio and

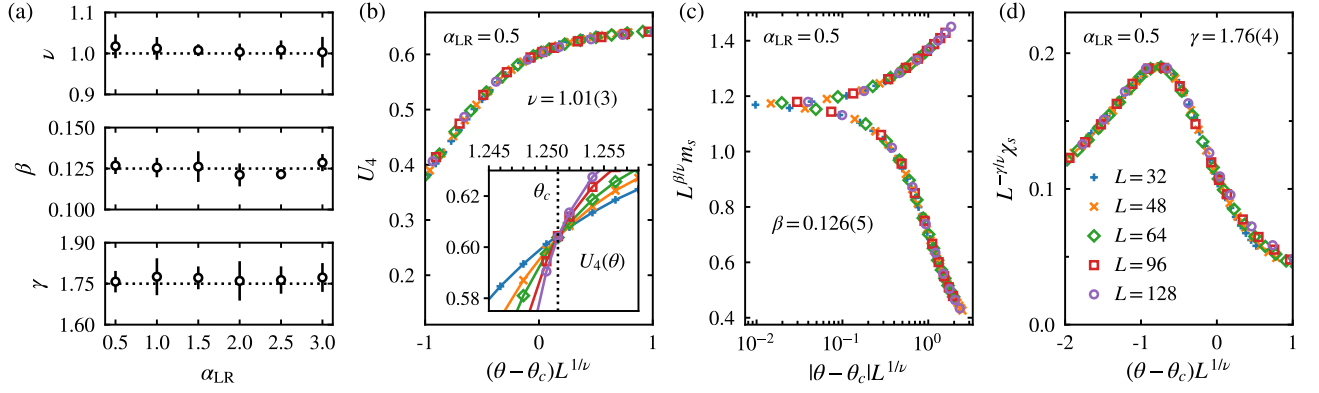


FIG. 2. FSS analysis of RBM observables. (a) The estimates of the critical exponents ν , β , γ are plotted in the range of α_{LR} between 0.5 and 3. The dotted lines are given for comparison with the SR Ising values. The FSS collapse tests with the critical exponents are demonstrated at $\alpha_{\text{LR}} = 0.5$ for the data of (b) the Binder's cumulant U_4 , (c) the AF order parameter m_s , and (d) the susceptibility χ_s . The inset of (b) shows the crossing point of U_4 locating the critical point θ_c .

the CFT description of the correlation function to examine the Ising criticality and the conformal invariance, respectively.

A. Order parameter and critical exponents

The emergence of the AF order can be detected by measuring the staggered magnetization in the input layer of the RBM. In the AF phase, the operator $\hat{M}_s = \sum_i (-1)^i \hat{\sigma}_i^x$ in each parity sector of the \mathbb{Z}_2 symmetry indicates a finite positive or negative expectation value. Although our MC sampling does not fix the parity, an alternative quantity $M_s(\mathbf{s}) = |\sum_i (-1)^i s_i|$ can characterize the order-disorder phase transition at the level of the RBM wave function. We write the order parameter as

$$m_s = \frac{1}{L} \langle M_s \rangle_{\text{mc}}. \quad (8)$$

Near a critical point θ_c , the order parameter measured in a finite system of size L is expected to behave asymptotically as $m_s(\theta, L) \sim L^{-\beta/\nu} \mathcal{M}_0^{(\pm)}(|\theta - \theta_c|L^{1/\nu})$ with the critical exponents β and ν , where $\mathcal{M}_0^{(\pm)}$ is a size-independent scaling function. The corresponding susceptibility can also be defined by the fluctuations of M_s as

$$\chi_s = \langle M_s^2 \rangle_{\text{mc}} - \langle M_s \rangle_{\text{mc}}^2, \quad (9)$$

which is expected to follow the FSS ansatz of $\chi_s(\theta, L) \sim L^{\gamma/\nu} \mathcal{X}_0[|\theta - \theta_c|L^{1/\nu}]$ associated with the exponent γ .

First we determine the critical point θ_c for a given α_{LR} by locating a crossing point of the Binder's fourth-order cumulant,

$$U_4 = 1 - \frac{\langle M_s^4 \rangle_{\text{mc}}}{3 \langle M_s^2 \rangle_{\text{mc}}^2}, \quad (10)$$

between the curves of different L 's. The FSS ansatz of the cumulant is given as $U_4(\theta, L) \sim \mathcal{U}_0[|\theta - \theta_c|L^{1/\nu}]$. Although \mathcal{U}_0 becomes independent of L for a large L , a finite-size correction can appear for small L 's. The finite-size correction

of the leading order is usually assumed to be in the form of $\theta_{L,2L}^* - \theta_c \propto L^{-\tilde{\omega}}$ for a crossing point $\theta_{L,2L}^*$ identified between two adjacent curves of system sizes L and $2L$. We determine θ_c based on this correction-to-scaling ansatz with the extrapolation to infinite size.

After locating the critical point θ_c , we estimate the critical exponents ν , β , and γ by performing the standard FSS analysis with the FSS ansatz of m_s , χ_s , and U_4 in the critical region. Figure 2 presents an example of the FSS analysis for $\alpha_{\text{LR}} = 0.5$, showing that the data points of different L 's fall well on a common scaling curve with our estimates of the critical exponents. The numerical estimates of the critical exponents and errors are measured using the PYFSSA package [72, 73]. We tabulate our estimate of θ_c and the critical exponents in Table I. Within the error bars, our estimates of the critical exponents are very close to the SR Ising values for all the values of α_{LR} examined as shown in Fig. 2(a), which is consistent with the previous DMRG results [58, 59].

B. Correlation function exponent

We also examine the critical exponent η of the correlation function. At the critical point θ_c given above in Sec. III A, we measure the spin-spin correlation function,

$$C_{xx}(r) = \langle \hat{\sigma}_i^x \hat{\sigma}_{i+r}^x \rangle = \langle s_i s_{i+r} \rangle_{\text{mc}}, \quad (11)$$

where the distance r runs from 1 to $L/2$ in the periodic chain, and this expression is independent of the site index i due to the translational symmetry imposed in our RBM wave function ansatz. The asymptotic algebraic decay of $C_{xx}(r) \propto r^{-\eta}$ expected at a critical point can be written for a finite system of length L as $C_{xx}(bL) \propto L^{-\eta}$ at $r = bL$, which is displayed for our choice of $b = 1/4$ in Fig. 3. We extract η from the linear fit of the data in the log-log plot. It turns out that the estimate of η is consistently smaller than the SR Ising value $1/4$ when α_{LR} decreases below 2, implying that the SR Ising criticality does not hold for $\alpha_{\text{LR}} < 2$. These observations are consistent

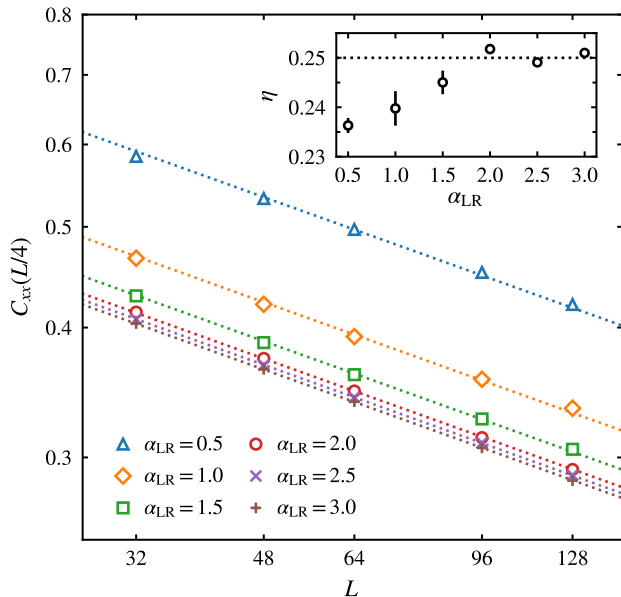


FIG. 3. Critical exponent of the spin-spin correlation function. The correlation function $C_{xx}(r)$ at $r = L/4$ is plotted as a function of the system size L . The inset shows the exponent η extracted from the data fitting to $C_{xx}(L/4) \propto L^{-\eta}$. The dotted lines given for comparison indicate the SR Ising exponent $\eta = 1/4$.

with the previous TDVP result [56], where the threshold at $\alpha_{LR} = 2.25$ was suggested.

However, it is worth noting that a change in η is connected to changes in the other exponents through the hyperscaling relations $\gamma/\nu = 2 - \eta$ and $2\beta/\nu = d + z - 2 + \eta$. The latter implies an apparent conflict between the previous TDVP and DMRG results [56, 58, 59]. The TDVP estimate of η decreases from $1/4$ for $\alpha_{LR} \lesssim 2$, whereas the DMRG studies reported $\nu \simeq 1$, $\beta \simeq 1/8$, and $z \simeq 1$. We have verified some of these critical exponents, but we cannot reconcile this conflict with the limited accuracy of our calculations. Thus, the exponents at the present accuracy may be unreliable to determine whether the Ising criticality of the SR limit survives or breaks down at a finite α_{LR} . This emphasizes the need for a test that does not rely on the estimates of the exponents.

C. Second Rényi entropy and central charge

The logarithmic system-size scaling of the entanglement entropy at a critical point in one dimension is a useful universal property to measure the central charge of the CFT that characterizes the phase transition [74–76]. In the previous estimate of the central charge using the TDVP [56], DMRG [57], and generalized Hatree-Fock [62] methods, the von Neumann entropy was examined under open boundary conditions (OBC). Instead, we consider the second Rényi entropy for the measurement using the RBM wave function under PBC. For the bipartition of a system into subsystems A and B , the Rényi

entropy of an order n for ρ_A is written as

$$S_n(\rho_A) = \frac{1}{1-n} \ln \text{tr} \rho_A^n, \quad (12)$$

where $\rho_A \equiv \text{tr}_B \rho$ is the reduced density matrix of A for a pure state ρ . The von Neumann entropy is recovered at the limit of $n = 1$. For the universality class fixed by the CFT, the von Neumann and Rényi entropies at the critical point indicate the same central charge c in the leading-order FSS behavior. For PBC, the asymptotic scaling behavior of S_n [76] for half-chain bipartition is written as

$$S_n = \frac{c}{6} \left(1 + \frac{1}{n}\right) \ln L + c'_n, \quad (13)$$

where c'_n is a nonuniversal constant.

The second Rényi entropy S_2 can be reliably measured in QMC calculations by using the replica trick [77], which has been successfully applied to the VMC calculations with the RBM wave function [15]. We consider only S_2 , but a method was proposed to compute S_n of the higher n and to approximate S_1 in a different NQS representation [78]. Measuring S_2 requires two copies of the RBM state, namely $\mathbf{s}^{(1)}$ and $\mathbf{s}^{(2)}$, sampled from the joint probability distribution $P(\mathbf{s}^{(1)}, \mathbf{s}^{(2)}) \propto |\Psi(\mathbf{s}^{(1)})|^2 |\Psi(\mathbf{s}^{(2)})|^2$. Each copy can be rewritten in a bipartite basis of $\mathbf{s} \equiv (\mathbf{s}_A, \mathbf{s}_B)$, where \mathbf{s}_A and \mathbf{s}_B are associated with the subsystems A and B . Then, one can obtain e^{-S_2} by measuring the swapping operator on A as

$$e^{-S_2} = \left\langle \frac{\Psi(\mathbf{s}_A^{(2)}, \mathbf{s}_B^{(1)}) \Psi(\mathbf{s}_A^{(1)}, \mathbf{s}_B^{(2)})}{\Psi(\mathbf{s}_A^{(1)}, \mathbf{s}_B^{(1)}) \Psi(\mathbf{s}_A^{(2)}, \mathbf{s}_B^{(2)})} \right\rangle_{\text{mc}}. \quad (14)$$

Figure 4(a) shows the measurements of S_2 for different L 's at the critical point. While the expected asymptotic behavior of $S_2(L) = \frac{c}{4} \ln L + c'_2$ is apparent, a finite-size correction that decays with increasing L may exist. To estimate c from the S_2 data of finite L 's, we define the effective central charge as

$$c_{\text{eff}}(L) = \frac{4}{\ln 2} [S_2(L) - S_2(L/2)], \quad (15)$$

where the central charge can be estimated by the extrapolation of $c_{\text{eff}}(L)$ to $L = \infty$ along a model curve of the finite-size behavior. According to the previous FSS analysis at a

α_{LR}	θ_c	ν	β	γ	η	c_∞
3.0	0.8714(7)	1.00(4)	0.128(5)	1.77(5)	0.2510(4)	0.496(5)
2.5	0.9041(6)	1.01(2)	0.122(3)	1.76(5)	0.2491(2)	0.500(4)
2.0	0.9489(7)	1.00(2)	0.121(7)	1.76(7)	0.2518(7)	0.502(5)
1.5	1.012(1)	1.00(1)	0.126(9)	1.77(4)	0.2450(24)	0.508(4)
1.0	1.103(1)	1.01(3)	0.126(6)	1.78(7)	0.2398(35)	0.490(5)
0.5	1.251(1)	1.01(3)	0.127(5)	1.76(4)	0.2363(15)	0.454(8)

TABLE I. List of the critical points and exponents. Critical exponents ν , β , and γ are determined in the FSS analysis of the collapse of the scaling curve. The exponent η is measured from the scaling of the spin-spin correlation function along a fixed $r/L = 1/4$ at the critical point θ_c . The central charge c_∞ is extracted from the logarithmic scaling of the second Rényi entropy.

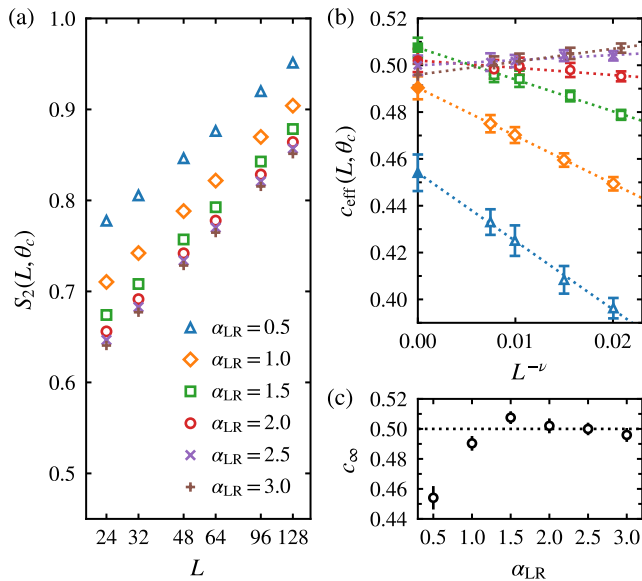


FIG. 4. Estimate of the central charge. (a) The second Rényi entropy S_2 of a half chain is plotted at the critical point θ_c as a function of system size L . (b) The effective central charge c_{eff} (empty symbols) is plotted as a function of $1/L$. Solid symbols and their error bars indicate our estimate of the central charge c_∞ and its standard error obtained from the linear fit (dotted lines) of the c_{eff} data. In (c), c_∞ is plotted as a function of α_{LR} .

second-order phase transition [79], the finite-size correction of S_2 would be proportional to $L^{-\nu}$ under PBC. Since Eq. (15) inherits the correction of S_2 , we fit the data to the line of $c_{\text{eff}}(L) = c_\infty + aL^{-\nu}$ as shown in Fig. 4(b), where the fitting parameter c_∞ is our estimate of the central charge.

In Fig. 4(c), the estimate of c_∞ for $\alpha_{\text{LR}} \lesssim 1$ indicate a deviation from $c = 1/2$ of the 2D Ising CFT. While such a deviation in the central charge was also previously observed for a similar range of α_{LR} [56, 57], it is worth noting that the direction of a deviation appears to vary depending on the types of entanglement entropy or boundary conditions. In the present work based on S_2 under PBC, we observe the decrease of c_∞ that goes below $1/2$ for a small α_{LR} . In contrast, the use of S_1 under OBC in the previous studies showed a large increase in central charge as α_{LR} decreases below 1.

So far, we have verified the previous TDVP and DMRG results on the critical exponents and the central charge [56–59]. However, questions remain about the Ising criticality and the conformal invariance. As discussed through the hyperscaling relations, we still need to go beyond the estimate of the critical exponents to see whether the 2D Ising universality class genuinely holds for any finite α_{LR} or if there is a criterion for how large α_{LR} should be to retain the criticality of the SR limit. On the other hand, the deviation of the central charge does not provide a sufficient condition to identify the breakdown of conformal invariance [66]. In the following sections, we thus provide additional stringent tests of the criticality change and the conformal invariance breakdown.

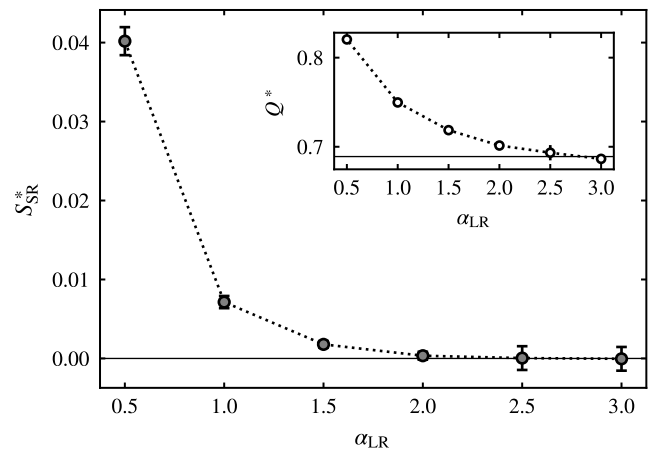


FIG. 5. Test of the critical Binder ratio. The self-combined ratio S_{SR}^* and the Binder ratio Q^* at the critical point are plotted as a function of α_{LR} . The data points are extrapolated to infinite size. The horizontal solid lines indicate the SR limit.

D. Critical Binder ratio

For an alternative test for the Ising criticality, we consider the Binder ratio, $Q \equiv \langle M_s^2 \rangle_{\text{mc}}^2 / \langle M_s^4 \rangle_{\text{mc}}$, of the second and fourth moments of the staggered magnetization. The Binder ratio at a critical point exhibits a particular value contributing to the universality of the critical behavior, while the value depends on the boundary conditions and the aspect ratio of the system (see, for instance, Refs. [80, 81] and references therein). The critical Binder ratio has been used as a reliable ingredient to identify the universality class in the classical long-range Ising model [42], which inspires us to perform the same test of how the Binder ratio depends on α_{LR} for the critical RBM wave function in the AF-LR-TFIC.

In the SR limit, at the exact critical point $\theta_c = \pi/4$, we obtain the value of $Q_{\text{SR}}^* = 0.689(4)$ from the power-law extrapolation of $Q(L)$ to infinite L . This particular value of the ratio has not previously been known for the AF-TFIC, but it turns out that the corresponding value of the cumulant $U_4^* = 0.516(3)$ is in good agreement with the previous MC estimate of $U_4^* = 0.514(1)$ reported in the classical 2D Ising model subject to the mixed boundary conditions where the system is periodic in one direction and open in the other direction [82]. The implicit connection between the mixed boundary conditions and the cylindrical geometry of our periodic chain under the imaginary-time evolution at zero temperature may expect the universal value of the Binder ratio in the SR limit.

For a finite α_{LR} , we consider the indicator called the self-combined Binder ratio proposed in Ref. [42],

$$S_{\text{SR}}(L) = \frac{1}{Q_{\text{SR}}^*} Q(L) + \frac{1}{Q(L)} Q_{\text{SR}}^* - 2, \quad (16)$$

which removes the leading-order finite-size correction in $Q(L)$ and thus exhibits better convergence with increasing L if an accurate value of Q_{SR}^* is provided. Figure 5 displays the value of $S_{\text{SR}}^* \equiv \lim_{L \rightarrow \infty} S_{\text{SR}}(L)$ obtained from the power-law extrapolation to infinite L . It turns out that while S_{SR}^* is almost

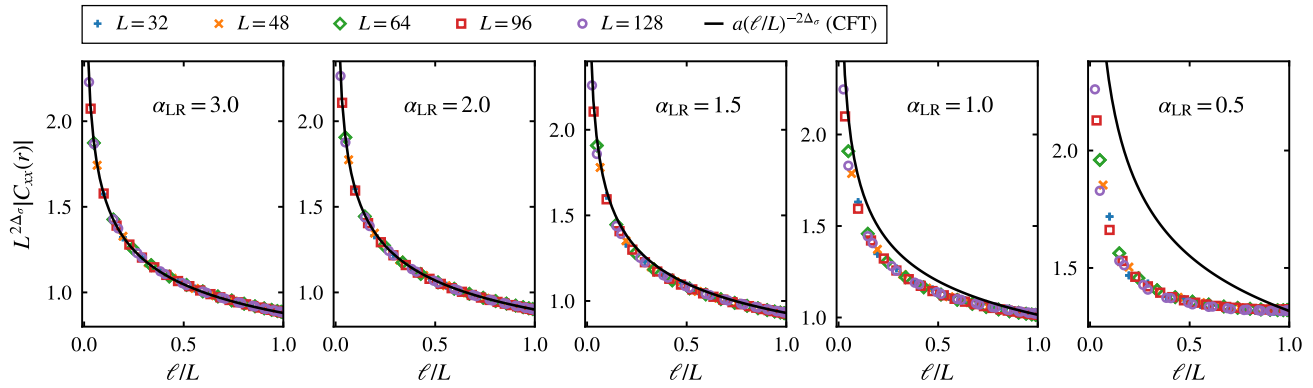


FIG. 6. FSS analysis of the spin-spin correlation function. The data collapse of $L^{2\Delta_\sigma} |C_{xx}(r)|$ is examined as a function of the scaled chord length $\ell/L \equiv \sin(\pi r/L)$ with the measured exponent $\eta = 2\Delta_\sigma$. The solid line indicates the CFT-predicted form of $a(\ell/L)^{-2\Delta_\sigma}$ given for comparison with the scaled curve of the measured correlation function.

zero for $\alpha_{LR} = 3$ and 2.5 , the deviation of S_{SR}^* appears for $\alpha_{LR} \lesssim 2$ and increases as α_{LR} decreases. The estimate of $Q^* \equiv \lim_{L \rightarrow \infty} Q(L)$ shows a similar increase from the value of the SR limit as α_{LR} decreases, although it still indicates a slight deviation even for $\alpha_{LR} = 2.5$ and 3 where $S_{SR}^* \approx 0$. This is consistent with the observation in Ref. [42], verifying that $S_{LR}(L)$ converges better at a finite L . Our data suggest that the threshold for the SR Ising criticality is possibly around $\alpha_{LR} = 2$ above which S_{SR}^* is zero within the error bars.

E. CFT test of the correlation function

We detect the breakdown of conformal invariance by identifying a mismatch between the measured correlation function and the CFT description, following the strategy of Ref. [66]. The CFT in a cylindrical space-time geometry restricts the scaling and functional form of the correlation functions [83, 84]. In the presence of conformal invariance at a critical point, the spin-spin correlation function in Eq. (11) must behave asymptotically as

$$C_{xx}(r) \propto \ell^{-2\Delta_\sigma} = \left[L \sin\left(\pi \frac{r}{L}\right) \right]^{-2\Delta_\sigma}, \quad (17)$$

where the scaling variable $\ell \equiv L \sin(\pi r/L)$ is the chord length, and the scaling dimension Δ_σ corresponds to a half of the decay exponent η . The test of Eq. (17) requires the estimate of the exponent $\eta = 2\Delta_\sigma$, which we have already measured in the FSS analysis of $C_{xx}(L/4) \propto L^{-\eta}$ along $r = L/4$ for different L 's in Sec. III B. Using the estimate of η obtained for each α_{LR} , we present how the measured C_{xx} deviates from the CFT form of Eq. (17) as α_{LR} changes.

Figure 6 shows a good FSS collapse of the data points of $L^{2\Delta_\sigma} |C_{xx}(r)|$ on a common scaling curve with the measured value of $\eta = 2\Delta_\sigma$, which is plotted as a function of ℓ/L . This allows us to make a graphical comparison with the CFT curve of $L^{2\Delta_\sigma} |C_{xx}(r)| \propto (\ell/L)^{-2\Delta_\sigma}$. We find that the deviation between the data and the CFT curve becomes pronounced for $\alpha_{LR} < 2$, indicating the breakdown of conformal invariance.

This observation also implies that the central charge is indeed unreliable in detecting the breakdown of conformal invariance because the deviation from the CFT curve already occurs in the range of $\alpha_{LR} > 1$ where the central charge is found to be very close to $1/2$.

A more quantitative CFT indicator can be provided by the scaled correlation function [66], which is the ratio between the measured correlation function and the CFT prediction,

$$C_{sc}(\ell/L) = \left[L \sin\left(\pi \frac{r}{L}\right) \right]^{2\Delta_\sigma} |C_{xx}(r)|. \quad (18)$$

In Fig. 7, we specify the measured value of $\eta = 2\Delta_\sigma$ for each α_{LR} examined. The appearance of a nonzero slope tail in the scaled correlation function C_{sc} signals the breakdown of conformal invariance. Our data shows that $C_{sc}(\ell/L)$ exhibits a tail that is almost linear in ℓ/L , which allows us to measure the slope from a straight-line fit of the tail part.

Figure 7 shows a notable increase in slope as α_{LR} decreases below 2, which justifies the graphical deviation of the data from the CFT curve in Fig. 6. However, for $2 \leq \alpha_{LR} \leq 3$, where the data and the CFT curve appear to match in Fig. 6, it turns out that the slope decreases with increasing α_{LR} but remains finite in the range of α_{LR} examined. This can be compared with the benchmark case of the SR limit, where the slope is near zero within the error bar. Although it is challenging to locate the threshold of the precise zero slope within the limited accuracy of our calculations, the nonvanishing slope raises the possibility that the breakdown threshold in the AF-LR-TFIC may differ from the threshold in the Kitaev chain, where the conformal symmetry was argued to be broken at $\alpha_{LR} = 2$ in the approximate renormalization group approach [65].

Accurate correlation function calculations on the power-law decaying tail are crucial to determine the threshold. However, apart from the common finite-size issues, our RBM wave function has its limitations in accuracy. The benchmark in the SR limit indicates the measured exponent $\eta = 0.2518(6)$ that is slightly deviated from the exact value $1/4$, implying a bias in the optimized wave function. Although increasing the number of filters n_h can enhance the expressivity and hence the accuracy of the RBM ansatz, our implementation is practically

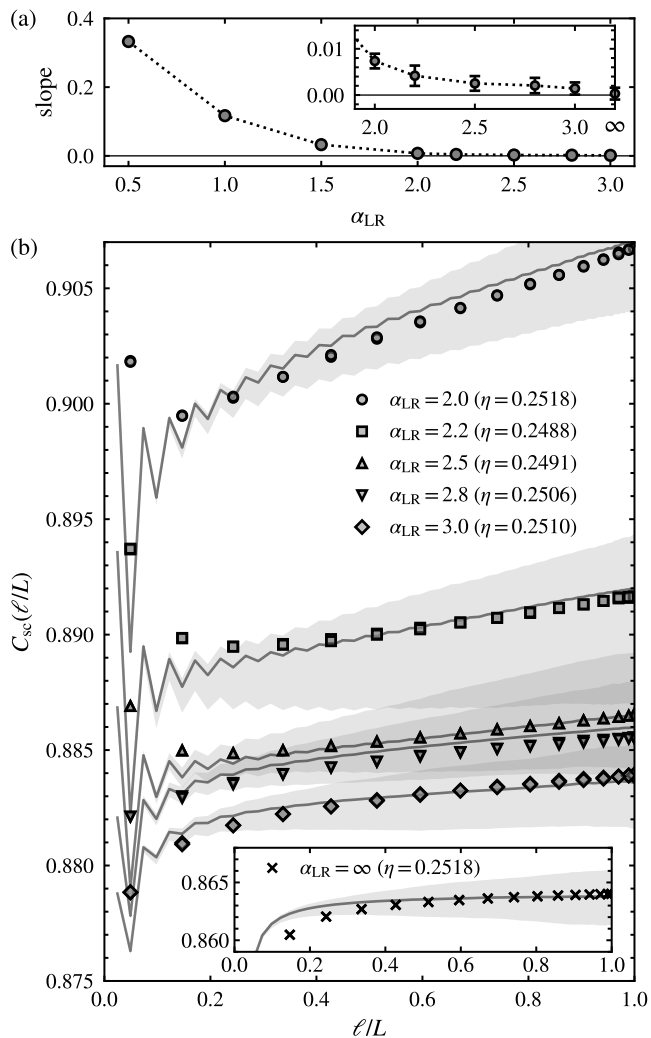


FIG. 7. The CFT test of the scaled correlation function. Equation (18) is examined using ten RBM wave function samples obtained from independent VMC optimizations at a critical point. (a) The slope of $C_{sc}(\ell/L)$ is measured from the straight-line fit to the data of $L = 128$ for $\ell/L > 0.6$. (b) The symbols indicate the data of $L = 64$ where the sample-to-sample fluctuations are smaller than the symbol size. The solid line is the average over the RBM samples for $L = 128$. The shade fills the area between the minimum and maximum magnitudes of the data in the RBM samples for $L = 128$.

limited to $n_h = 16$ due to the computational time costs for the FSS analysis. Moreover, because of the same time costs, only a few samples of the optimized RBM wave function are generated to measure fluctuations across independent VMC optimizations. These sample-to-sample fluctuations tend to increase with the system size and cause a significant uncertainty in the scaled correlation function for $L = 128$, as shown in Fig. 7(b). These practical limitations pose numerical challenges for our VMC+RBM simulations to find the precise breakdown threshold of conformal invariance.

IV. SUMMARY AND CONCLUSIONS

We have investigated criticality and conformal invariance at a quantum phase transition in the AF-LR-TFIC using the VMC calculations with the RBM trial wave function ansatz. Our main findings are from the tests of the universal Binder ratio [42] and the CFT description of the spin-spin correlation function [66]. The critical Binder ratio exhibits an increasing deviation from the universal ratio of the SR limit when α_{LR} decreases below 2, implying that the criticality for $\alpha_{LR} < 2$ is different from the 2D Ising class. On the other hand, in the test of the correlation function, we found evidence of the conformal invariance breakdown from the deviation between the form of the correlation function and the CFT description. The deviation from the CFT description becomes more pronounced as α_{LR} decreases, although the precise threshold of the breakdown is yet to be determined.

These findings present progress in characterizing the phase transition in the AF-LR-TFIC beyond the observations of the critical exponents and the central charge. In the FSS analysis to extract the critical exponents, we observed that the exponents ν , β , and γ are very close to the SR Ising exponents for the examined range of $0.5 \leq \alpha_{LR} \leq 3$. In contrast, the decay exponent η of the correlation function and the central charge extracted from the second Rényi entropy differ from the SR Ising values when α_{LR} becomes small enough. Although these observations are consistent with the previous TDVP and DMRG calculations [56–59], the central charge is insufficient to diagnose the conformal invariance breakdown [66], and the critical exponent estimates in the present accuracy are inconclusive on the change of the criticality.

Our VMC+RBM calculations have demonstrated the practical applicability of the NQS framework for studying quantum phase transitions. However, there are also unsolved issues in our calculations that need further numerical advancement. Finding the precise breakdown threshold of conformal invariance needs high-precision calculations of the correlation function or more sensitive indicators of conformal symmetry, such as Klein bottle entropy [85]. In addition, the apparent mismatches between the correlation function exponent and the other critical exponents need careful investigation to examine their hyperscaling relations with higher numerical accuracy.

ACKNOWLEDGMENTS

J.K. and D.K. contributed equally to this work. We thank Syngye Todo and Hong-Hao Tu for the fruitful discussions during the ASG meeting at the PCS-IBS. This work was supported by the Basic Science Research Program through the National Research Foundation of Korea (NRF-2019R1F1A106321) and also by the KIAS associate member program. Computing resources are provided by the KISTI supercomputing center (KSC-2021-CRE-0165). We appreciate APCTP and PCS-IBS for their hospitality during the completion of this work.

- [1] G. Carleo, I. Cirac, K. Cranmer, L. Daudet, M. Schuld, N. Tishby, L. Vogt-Maranto, and L. Zdeborová, Machine learning and the physical sciences, *Rev. Mod. Phys.* **91**, 045002 (2019).
- [2] J. Carrasquilla, Machine learning for quantum matter, *Adv. Phys.* **5**, 1797528 (2020).
- [3] J. Carrasquilla and G. Torlai, How to use neural networks to investigate quantum many-body physics, *PRX Quantum* **2**, 040201 (2021).
- [4] A. Dawid, J. Arnold, B. Reuena, A. Gresch, M. Płodzień, K. Donatella, K. A. Nicoli, P. Stornati, R. Koch, M. Büttner, R. Okuła, G. Muñoz-Gil, R. A. Vargas-Hernández, A. Cervera-Lierta, J. Carrasquilla, V. Dunjko, M. Gabrié, P. Huembeli, E. van Nieuwenburg, F. Vicentini, L. Wang, S. J. Wetzel, G. Carleo, E. Greplová, R. Krems, F. Marquardt, M. Tomza, M. Lewenstein, and A. Dauphin, Modern applications of machine learning in quantum sciences, arXiv:2204.04198.
- [5] G. Carleo and M. Troyer, Solving the quantum many-body problem with artificial neural networks, *Science* **355**, 602 (2017).
- [6] Y. Nomura, A. S. Darmawan, Y. Yamaji, and M. Imada, Restricted Boltzmann machine learning for solving strongly correlated quantum systems, *Phys. Rev. B* **96**, 205152 (2017).
- [7] H. Saito, Solving the bose-hubbard model with machine learning, *J. Phys. Soc. Jpn.* **86**, 093001 (2017).
- [8] M. Schmitt and M. Heyl, Quantum many-body dynamics in two dimensions with artificial neural networks, *Phys. Rev. Lett.* **125**, 100503 (2020).
- [9] M. Schmitt, M. M. Rams, J. Dziarmaga, M. Heyl, and W. H. Zurek, Quantum phase transition dynamics in the two-dimensional transverse-field ising model, *Sci. Adv.* **8**, eabl6850 (2022).
- [10] K. Donatella, Z. Denis, A. Le Boité, and C. Ciuti, Dynamics with autoregressive neural quantum states: Application to critical quench dynamics, *Phys. Rev. A* **108**, 022210 (2023).
- [11] A. Nagy and V. Savona, Variational quantum monte carlo method with a neural-network ansatz for open quantum systems, *Phys. Rev. Lett.* **122**, 250501 (2019).
- [12] M. J. Hartmann and G. Carleo, Neural-network approach to dissipative quantum many-body dynamics, *Phys. Rev. Lett.* **122**, 250502 (2019).
- [13] F. Vicentini, A. Biella, N. Regnault, and C. Ciuti, Variational neural-network ansatz for steady states in open quantum systems, *Phys. Rev. Lett.* **122**, 250503 (2019).
- [14] N. Yoshioka and R. Hamazaki, Constructing neural stationary states for open quantum many-body systems, *Phys. Rev. B* **99**, 214306 (2019).
- [15] G. Torlai, G. Mazzola, J. Carrasquilla, M. Troyer, R. Melko, and G. Carleo, Neural-network quantum state tomography, *Nature Phys.* **14**, 447 (2018).
- [16] G. Torlai, B. Timar, E. P. L. van Nieuwenburg, H. Levine, A. Omran, A. Keesling, H. Bernien, M. Greiner, V. Vuletić, M. D. Lukin, R. G. Melko, and M. Endres, Integrating neural networks with a quantum simulator for state reconstruction, *Phys. Rev. Lett.* **123**, 230504 (2019).
- [17] Y. Nomura and M. Imada, Dirac-type nodal spin liquid revealed by refined quantum many-body solver using neural-network wave function, correlation ratio, and level spectroscopy, *Phys. Rev. X* **11**, 031034 (2021).
- [18] A. Chen, K. Choo, N. Astrakhantsev, and T. Neupert, Neural network evolution strategy for solving quantum sign structures, *Phys. Rev. Res.* **4**, L022026 (2022).
- [19] A. Szabó and C. Castelnovo, Neural network wave functions and the sign problem, *Phys. Rev. Res.* **2**, 033075 (2020).
- [20] T. Westerhout, N. Astrakhantsev, K. S. Tikhonov, M. I. Katsnelson, and A. A. Bagrov, Generalization properties of neural network approximations to frustrated magnet ground states, *Nat. Commun.* **11**, 1593 (2020).
- [21] F. Ferrari, F. Becca, and J. Carrasquilla, Neural gutzwiller-projected variational wave functions, *Phys. Rev. B* **100**, 125131 (2019).
- [22] K. Choo, T. Neupert, and G. Carleo, Two-dimensional frustrated J_1-J_2 model studied with neural network quantum states, *Phys. Rev. B* **100**, 125124 (2019).
- [23] X. Liang, W.-Y. Liu, P.-Z. Lin, G.-C. Guo, Y.-S. Zhang, and L. He, Solving frustrated quantum many-particle models with convolutional neural networks, *Phys. Rev. B* **98**, 104426 (2018).
- [24] K. Choo, A. Mezzacapo, and G. Carleo, Fermionic neural-network states for ab-initio electronic structure, *Nat. Commun.* **11**, 2368 (2020).
- [25] D. Pfau, J. S. Spencer, A. G. D. G. Matthews, and W. M. C. Foulkes, Ab initio solution of the many-electron schrödinger equation with deep neural networks, *Phys. Rev. Res.* **2**, 033429 (2020).
- [26] J. Hermann, Z. Schätzle, and F. Noé, Deep-neural-network solution of the electronic Schrödinger equation, *Nat. Chem.* **12**, 891 (2020).
- [27] D.-L. Deng, X. Li, and S. Das Sarma, Quantum entanglement in neural network states, *Phys. Rev. X* **7**, 021021 (2017).
- [28] J. Chen, S. Cheng, H. Xie, L. Wang, and T. Xiang, Equivalence of restricted Boltzmann machines and tensor network states, *Phys. Rev. B* **97**, 085104 (2018).
- [29] I. Glasser, N. Pancotti, M. August, I. D. Rodriguez, and J. I. Cirac, Neural-network quantum states, string-bond states, and chiral topological states, *Phys. Rev. X* **8**, 011006 (2018).
- [30] Y. Levine, O. Sharir, N. Cohen, and A. Shashua, Quantum entanglement in deep learning architectures, *Phys. Rev. Lett.* **122**, 065301 (2019).
- [31] O. Sharir, A. Shashua, and G. Carleo, Neural tensor contractions and the expressive power of deep neural quantum states, *Phys. Rev. B* **106**, 205136 (2022).
- [32] N. Defenu, T. Donner, T. Macrì, G. Pagano, S. Ruffo, and A. Trombettoni, Long-range interacting quantum systems, *Rev. Mod. Phys.* **95**, 035002 (2023).
- [33] C. Monroe, W. C. Campbell, L.-M. Duan, Z.-X. Gong, A. V. Gorshkov, P. W. Hess, R. Islam, K. Kim, N. M. Linke, G. Pagano, P. Richerme, C. Senko, and N. Y. Yao, Programmable quantum simulations of spin systems with trapped ions, *Rev. Mod. Phys.* **93**, 025001 (2021).
- [34] R. Islam, E. E. Edwards, K. Kim, S. Korenblit, C. Noh, H. Carmichael, G.-D. Lin, L.-M. Duan, C.-C. Joseph Wang, J. K. Freericks, and C. Monroe, Onset of a quantum phase transition with a trapped ion quantum simulator, *Nat. Commun.* **2**, 377 (2011).
- [35] J. Zhang, G. Pagano, P. W. Hess, A. Kyprianidis, P. Becker, H. Kaplan, A. V. Gorshkov, Z.-X. Gong, and C. Monroe, Observation of a many-body dynamical phase transition with a 53-qubit quantum simulator, *Nature* **551**, 601 (2017).
- [36] B.-W. Li, Y.-K. Wu, Q.-X. Mei, R. Yao, W.-Q. Lian, M.-L. Cai, Y. Wang, B.-X. Qi, L. Yao, L. He, Z.-C. Zhou, and L.-M. Duan, Probing critical behavior of long-range transverse-field Ising model through quantum Kibble-Zurek mechanism, *PRX Quantum* **4**, 010302 (2023).

- [37] S. Sachdev, *Quantum Phase Transitions*, 2nd ed. (Cambridge University Press, New York, 2011).
- [38] N. Defenu, A. Codello, S. Ruffo, and A. Trombettoni, Criticality of spin systems with weak long-range interactions, *J. Phys. A: Math. Theor.* **53**, 143001 (2020).
- [39] J. Sak, Recursion relations and fixed points for ferromagnets with long-range interactions, *Phys. Rev. B* **8**, 281 (1973).
- [40] E. Luijten and H. W. J. Blöte, Boundary between long-range and short-range critical behavior in systems with algebraic interactions, *Phys. Rev. Lett.* **89**, 025703 (2002).
- [41] M. C. Angelini, G. Parisi, and F. Ricci-Tersenghi, Relations between short-range and long-range Ising models, *Phys. Rev. E* **89**, 062120 (2014).
- [42] T. Horita, H. Suwa, and S. Todo, Upper and lower critical decay exponents of Ising ferromagnets with long-range interaction, *Phys. Rev. E* **95**, 012143 (2017).
- [43] C. Behan, L. Rastelli, S. Rychkov, and B. Zan, Long-range critical exponents near the short-range crossover, *Phys. Rev. Lett.* **118**, 241601 (2017).
- [44] A. W. Sandvik, Ground states of a frustrated quantum spin chain with long-range interactions, *Phys. Rev. Lett.* **104**, 137204 (2010).
- [45] S. Fey, S. C. Kapfer, and K. P. Schmidt, Quantum criticality of two-dimensional quantum magnets with long-range interactions, *Phys. Rev. Lett.* **122**, 017203 (2019).
- [46] J. Koziol, S. Fey, S. C. Kapfer, and K. P. Schmidt, Quantum criticality of the transverse-field Ising model with long-range interactions on triangular-lattice cylinders, *Phys. Rev. B* **100**, 144411 (2019).
- [47] S. Humeniuk, Thermal Kosterlitz–Thouless transitions in the $1/r^2$ long-range ferromagnetic quantum Ising chain revisited, *J. Stat. Mech.* **2020**, 063105.
- [48] M. F. Paulos, S. Rychkov, B. C. van Rees, and B. Zan, Conformal invariance in the long-range Ising model, *Nucl. Phys. B* **902**, 246 (2016).
- [49] A. Dutta and J. K. Bhattacharjee, Phase transitions in the quantum Ising and rotor models with a long-range interaction, *Phys. Rev. B* **64**, 184106 (2001).
- [50] M. Knap, A. Kantian, T. Giamarchi, I. Bloch, M. D. Lukin, and E. Demler, Probing real-space and time-resolved correlation functions with many-body Ramsey interferometry, *Phys. Rev. Lett.* **111**, 147205 (2013).
- [51] N. Defenu, A. Trombettoni, and S. Ruffo, Criticality and phase diagram of quantum long-range $O(N)$ models, *Phys. Rev. B* **96**, 104432 (2017).
- [52] A. Langheld, J. A. Koziol, P. Adelhardt, S. C. Kapfer, and K. P. Schmidt, Scaling at quantum phase transitions above the upper critical dimension, *SciPost Phys.* **13**, 088 (2022).
- [53] Z. Zhu, G. Sun, W.-L. You, and D.-N. Shi, Fidelity and criticality of a quantum Ising chain with long-range interactions, *Phys. Rev. A* **98**, 023607 (2018).
- [54] S. Shiratani and S. Todo, Stochastic approximation analysis of dynamical quantum critical phenomena in long-range transverse-field Ising chain, arXiv:2305.14121.
- [55] J. Ren, Z. Wang, W. Chen, and W.-L. You, Long-range order and quantum criticality in antiferromagnetic chains with long-range staggered interactions, *Phys. Rev. E* **105**, 034128 (2022).
- [56] T. Koffel, M. Lewenstein, and L. Tagliacozzo, Entanglement entropy for the long-range Ising chain in a transverse field, *Phys. Rev. Lett.* **109**, 267203 (2012).
- [57] D. Vodola, L. Lepori, E. Ercolessi, and G. Pupillo, Long-range Ising and Kitaev models: phases, correlations and edge modes, *New J. Phys.* **18**, 015001 (2016).
- [58] G. Sun, Fidelity susceptibility study of quantum long-range antiferromagnetic Ising chain, *Phys. Rev. A* **96**, 043621 (2017).
- [59] R. Puebla, O. Marty, and M. B. Plenio, Quantum Kibble-Zurek physics in long-range transverse-field Ising models, *Phys. Rev. A* **100**, 032115 (2019).
- [60] S. Fey and K. P. Schmidt, Critical behavior of quantum magnets with long-range interactions in the thermodynamic limit, *Phys. Rev. B* **94**, 075156 (2016).
- [61] J. A. Koziol, A. Langheld, S. C. Kapfer, and K. P. Schmidt, Quantum-critical properties of the long-range transverse-field Ising model from quantum Monte Carlo simulations, *Phys. Rev. B* **103**, 245135 (2021).
- [62] M. P. Kaicher, D. Vodola, and S. B. Jäger, Mean-field treatment of the long-range transverse field Ising model with fermionic gaussian states, *Phys. Rev. B* **107**, 165144 (2023).
- [63] J. C. Halimeh, M. Van Damme, L. Guo, J. Lang, and P. Hauke, Dynamical phase transitions in quantum spin models with antiferromagnetic long-range interactions, *Phys. Rev. B* **104**, 115133 (2021).
- [64] D. Vodola, L. Lepori, E. Ercolessi, A. V. Gorshkov, and G. Pupillo, Kitaev chains with long-range pairing, *Phys. Rev. Lett.* **113**, 156402 (2014).
- [65] L. Lepori, D. Vodola, G. Pupillo, G. Gori, and A. Trombettoni, Effective theory and breakdown of conformal symmetry in a long-range quantum chain, *Ann. Phys.* **374**, 35 (2016).
- [66] P. Patil, Y. Tang, E. Katz, and A. W. Sandvik, Indicators of conformal field theory: Entanglement entropy and multiple-point correlators, *Phys. Rev. B* **96**, 045140 (2017).
- [67] T. Kuwahara and K. Saito, Area law of noncritical ground states in 1D long-range interacting systems, *Nat. Commun.* **11**, 4478 (2020).
- [68] C.-Y. Park and M. J. Kastoryano, Expressive power of complex-valued restricted Boltzmann machines for solving nonstoquastic Hamiltonians, *Phys. Rev. B* **106**, 134437 (2022).
- [69] S. Sorella, Generalized lanczos algorithm for variational quantum monte carlo, *Phys. Rev. B* **64**, 024512 (2001).
- [70] S. Sorella, M. Casula, and D. Rocca, Weak binding between two aromatic rings: Feeling the van der Waals attraction by quantum Monte Carlo methods, *J. Chem. Phys.* **127**, 014105 (2007).
- [71] E. Neuscamman, C. J. Umrigar, and G. K.-L. Chan, Optimizing large parameter sets in variational quantum monte carlo, *Phys. Rev. B* **85**, 045103 (2012).
- [72] A. Sorge, pyfssa 0.7.6. zenodo (2015).
- [73] O. Melchert, autoscale.py - a program for automatic finite-size scaling analyses: A user's guide, arXiv:0910.5403.
- [74] G. Vidal, J. I. Latorre, E. Rico, and A. Kitaev, Entanglement in quantum critical phenomena, *Phys. Rev. Lett.* **90**, 227902 (2003).
- [75] P. Calabrese and J. Cardy, Entanglement entropy and quantum field theory, *J. Stat. Mech.* **2004**, P06002.
- [76] P. Calabrese and J. Cardy, Entanglement entropy and conformal field theory, *J. Phys. A: Math. Theor.* **42**, 504005 (2009).
- [77] M. B. Hastings, I. González, A. B. Kallin, and R. G. Melko, Measuring Rényi entanglement entropy in quantum Monte Carlo simulations, *Phys. Rev. Lett.* **104**, 157201 (2010).
- [78] Z. Wang and E. J. Davis, Calculating Rényi entropies with neural autoregressive quantum states, *Phys. Rev. A* **102**, 062413 (2020).
- [79] M. Campostrini, A. Pelissetto, and E. Vicari, Finite-size scaling at quantum transitions, *Phys. Rev. B* **89**, 094516 (2014).
- [80] V. Privman, *Finite Size Scaling and Numerical Simulation of Statistical Systems* (World Scientific, Singapore, 1990).
- [81] W. Selke, The critical Binder cumulant for isotropic Ising models on square and triangular lattices, *J. Stat. Mech.* **2007**, P04008.
- [82] W. Selke, Critical Binder cumulant of two-dimensional Ising models, *Eur. Phys. J. B* **51**, 223–228 (2006).

- [83] M. Henkel, *Conformal Invariance and Critical Phenomena* (Springer-Verlag, Berlin Heidelberg, 1999).
- [84] P. Francesco, P. Mathieu, and D. Sénéchal, *Conformal Field Theory* (Springer Science & Business Media, New York, 2012).
- [85] H.-H. Tu, Universal entropy of conformal critical theories on a Klein bottle, *Phys. Rev. Lett.* **119**, 261603 (2017).